

Measurement of somatosensory evoked magnetic fields using an adjustable magnetoresistive sensor array



Tetsuro Tatsuoka^{a,*},^{1,2}, Shigenori Kawabata^{b,3}, Jun Hashimoto^{b,4}, Yuko Hoshino^{b,5},
Kensuke Sekihara^{b,6}, Tomohiko Shibuya^{a,7}, Yoshiaki Adachi^{c,8}, Atsushi Okawa^{b,9}

^a TDK Corporation, Tokyo, Japan

^b Tokyo Medical and Dental University, Tokyo, Japan

^c Kanazawa Institute of Technology, Ishikawa, Japan

ARTICLE INFO

Keywords:

Biomagnetic sensors
Magnetoencephalography
Magnetoresistive element
Somatosensory evoked magnetic fields

ABSTRACT

An adjustable helmet-style magnetoresistive (MR) sensor array with room-temperature magnetic flux sensors was developed to demonstrate the simultaneous multipoint measurement of the somatosensory evoked magnetic field (SEF). Utilizing the extended sensor length, we designed the array to permit individual radial adjustment of each sensor, thereby achieving a precise fit to the varied head geometries of different subjects. Furthermore, the geometry of the sensor array precisely adjusted for the individual subject was quickly obtained by calibration. The SEF was measured in three healthy subjects using an array of 30-channel MR sensors placed on the left hemisphere of the head with median nerve stimulation in the right wrist and averaged over 8000 measurements. An M20 component considered to originate from the primary somatosensory cortex was observed at an approximate latency of 20 ms of the magnetic field waveform in all cases (maximum amplitude of 725 ± 257 fT, peak latency of 20.5 ± 0.45 ms). The phase inversion observed around C3 in the international 10–20 system corresponded to the palmar area of the primary somatosensory cortex on the contour map of the magnetic field at the M20 peak. The MR sensor, an affordable and easy-to-use magnetic sensor that does not require a zero-field environment nor a cryogenic apparatus, was successfully used for simultaneous multipoint SEF measurements in humans and provides a promising system for realizing magnetoencephalography application devices.

1. Introduction

Magnetoencephalography (MEG), which records weak magnetic fields derived from electrical activity in the brain, has been widely used in clinical applications such as focal epilepsy and brain science research as it demonstrates excellent temporal and spatial resolution and can noninvasively identify active areas from outside the body [1–3]. Conventional magnetoencephalographs (MEGs) use superconducting

quantum interference device (SQUID) magnetometers as magnetic sensors, which require cooling with liquid helium, resulting in high equipment and maintenance costs [4,5]. MEG or evoked MEG, which relies on room-temperature magnetic sensors such as optical pumping magnetometers (OPMs) or tunnel magnetoresistance (TMR) sensors, was recently reported [6,7]. Room-temperature magnetic sensors offer a high degree of freedom in terms of arrangement as they do not require a cryostat to store liquid helium. The sensors are placed in close contact

* Corresponding author.

E-mail address: tatsuoka@metool.co.jp (T. Tatsuoka).

¹ 0000-0003-1917-5823

² Is currently with METOOL Inc., Tokyo, Japan

³ 0000-0003-4687-7230

⁴ 0000-0002-1433-7144

⁵ 0000-0002-3501-0810

⁶ 0000-0002-2048-3797

⁷ 0009-0001-1349-3233

⁸ 0000-0002-9041-6987

⁹ 0000-0003-0227-8658

with each participant. As the magnetic field originating from the magnetic source decays with the square of the distance, shortening the distance from the signal source improves signal-to-noise ratio [8,9]. The magnetic sensor developed in this research utilizes the magnetoresistive (MR) effect. OPMs have a higher signal-to-noise ratio compared to that of the MR sensor used in this study; however, the MR sensor is superior in terms of cost, usability, and power consumption when compared with OPMs, as discussed further in Section 4.

Cases in which the M20 component of SEF was measured using MR sensors have been reported; however, the recordings were obtained with a single TMR sensor rather than simultaneous multisite measurements [6], or a personalized whole-head mask was used instead of an adjustable sensor array [10]. In this study, we conducted simultaneous multipoint measurements of the somatosensory evoked magnetic field (SEF) using a sensor array consisting of multiple magnetic sensors. The device utilizes MR effect elements and an adjustable fixture that allows the sensors to be positioned in close contact with the head.

2. Method

The SEF was measured in a magnetically shielded room (MSR) using a helmet-shaped sensor array with 30 MR sensors (Nivio xMR sensor, TDK, Tokyo, Japan). Fig. 1 shows the appearance and noise density spectrum of the magnetic sensor, and Table 1 lists the main characteristics of the MR sensor. The sensor had a cuboidal shape, 12-mm square, and 74 mm in length, with a noise density ranging from $3 \text{ pT Hz}^{-0.5}$ at 1 Hz. The MR element is a giant magnetoresistive (GMR) element. The sensitivity axis of the sensor was located along the longitudinal direction of the cuboid, and the magnetic field was recorded in the positive direction from the end face of the sensor to the cable. The sensor consisted of a four-element Wheatstone bridge to reduce the influence of temperature drift. Inside the sensor, a rod-shaped ferrite flux concentrator was magnetically coupled with the MR elements to improve the sensitivity. A compensating coil was wound around the flux concentrator to expand the dynamic range and improve the linearity through feedback control. The structure that realizes a compact magnetic sensor is patented [11].

The sensor array is characterized by a structure wherein multiple sensors are radially mounted on a helmet-shaped sensor holder fixed on an aluminum frame. The position of each sensor can be adjusted in the radial direction. The internal dimensions of the sensor holder were 188 mm in the left-right direction, 104 mm in the superior-inferior direction, and 238 mm in the anterior-posterior direction. The position of each sensor could be adjusted within approximately 20 mm by sliding it along the axial direction inside the cylindrical structure attached to the helmet-type sensor holder. The sensor's position could be fixed using immovable grub screws located at four points on the side as shown in Fig. 2. Thirty sensors were placed corresponding to the left hemisphere from the top of the head, such that the center was near C3 in the international 10–20 system as shown in Fig. 3. The sensors are positioned at an interval of approximately 30 mm to prevent crosstalk effects.

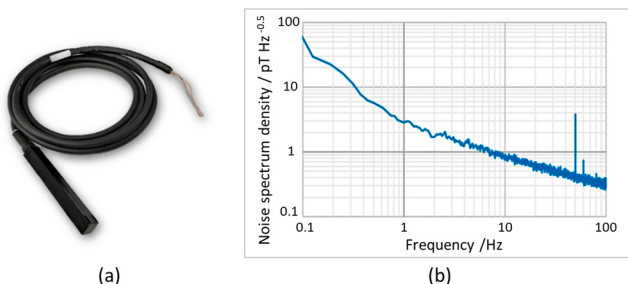


Fig. 1. (a) Appearance of the magnetic sensor, Nivio xMR sensor, BMS-SENSOR-05, TDK Corporation. (b) Noise characteristics. A noise level of $3 \text{ pT Hz}^{-0.5}$ at 1 Hz was achieved by using a flux concentrator.

Table 1
Characteristics of the MR sensor.

Item	Characteristics
Noise level	$3 \text{ pT Hz}^{-0.5}$ @ 1 Hz
Sensitivity	$87 \mu\text{V/nT}$
Dynamic range	$\pm 45 \mu\text{T}$
Frequency range	0.1 Hz to 10 kHz
Dimensions	$12 \times 12 \times 74 \text{ mm}$
Weight	20 g (sensor head), 100 g (cable)
MR element	GMR
MR ratio	10.5%

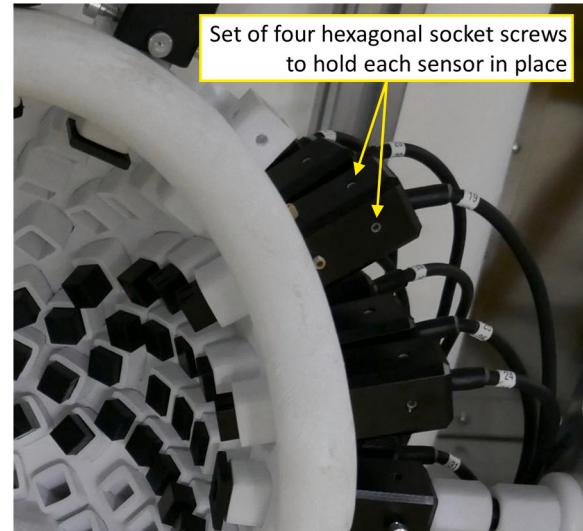


Fig. 2. Mechanism of sensor adjustment. Each sensor was moved in the radial direction and fixed with a screw.

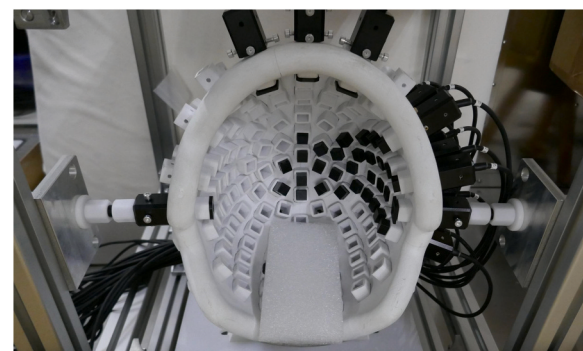


Fig. 3. Appearance and structure of the entire sensor array. Thirty MR sensors were installed at a position corresponding to the left hemisphere from the parietal of the cerebrum in a helmet-shaped sensor holder attached to an aluminum frame.

Magnetic field signals were recorded using a 24-bit A/D conversion unit (NI-9202, NI, Texas, US) and an electrical stimulator (Neuropack S1, MEB-9402, Nihon Kohden, Tokyo, Japan). The sensitivity, position, and orientation of each sensor were determined using a spherical calibration coil [12], which was originally designed for the SQUID-based whole-head MEG.

The room wherein the measurements were conducted was magnetically shielded by two layers of permalloy and two layers of aluminum with an attenuation of -32 dB at 1 Hz.

The subjects wore marker coils at five points, which were located at the center of the forehead, 4 cm at either side of this point, at the tragus

of the left ear, and at the nasion, to identify the position of the head relative to the sensor array; further, their heads were inserted into the sensor array in the supine position, as shown in Fig. 4. The operator adjusted the sensor positions such that all sensor tips were in close contact with the subjects' heads. The median nerve was electrically stimulated at the right wrist joint in three healthy male subjects, and the SEF was measured from the area centered around C3 of the international 10–20 system, the contralateral side of the stimulation (with an averaging count of 8000). The demographic data of the participants are presented in Table 2. Gender and age bias do not affect the validity of this study because the purpose of this study is to demonstrate that SEF can be measured by MR sensors located close to the subject's head using the developed array. Additionally, the M20 component of the SEF is not affected by mental activity or other physiological conditions, similar to the N20 component of somatosensory evoked potential (SEP), which is also used for intraoperative monitoring and electrophysiological monitoring in intensive care units. The measurement and signal processing conditions are listed in Tables 3 to 5. The filter settings were decided referring to the recommendation from the International Federation of Clinical Neurophysiology (IFCN) for SEP [13], with high-pass filtering below 3 Hz and low-pass filtering of 2 kHz or higher.

After the SEF measurement, a sinusoidal current was applied to the marker coils to generate a known magnetic field. The sensor array detected the magnetic field from the marker coils, whose positions were estimated via magnetic source analysis to reveal the position and orientation of the subject's head relative to the sensor array [14]. Upon completion of the measurements, the subject removed their head from the helmet, and the calibration coils were placed in the helmet. Magnetic field signals from the calibration coils were recorded, whereupon the 3D position coordinates of each sensor were identified based on the calibration coil. The position of the marker coil was estimated based on the information about the sensor position. The method for identifying the positions of the marker coils using the system calibration is detailed in [12]. For validation, a SEF measurement using a conventional SQUID-based biomagnetometer [15] was also conducted under the same stimulus conditions for one of the subjects.

3. Results

The SEF measurement results from the three subjects are shown in Fig. 7. The plot on the left indicates superimposed waveforms of magnetic field signals from all sensors. The plots in the middle show the waveforms of the sensors that included the highest positive/negative peaks around a latency of 20 ms. The peak at about 20 ms in latency was observed in all three subjects. The latency and amplitude of the peak were 20.5 ± 0.45 ms and 725 ± 257 fT, respectively. It should be noted that waveforms with a peak around 20 ms were not obtained when measurements were obtained using a stimulus of 0 mA, nor when



Fig. 4. Measuring scene. Subjects inserted their heads into the sensor array in the supine position.

Table 2

Demographic data of subjects.

Demographic data	Values
Number of subjects (n)	3
Age (year)	53.7 ± 7.4^a
Height (cm)	168 ± 6.2^a
Weight (kg)	66.3 ± 6.4^a
Handedness	Right: left, 3: 0

^a Data are expressed as the mean \pm standard deviation (SD).

Table 3

Recording conditions.

Recording conditions	Values
Number of channels	30 ch
High-pass filter	2 Hz (6 dB/oct)
Low-pass filter	2 kHz (-6 dB/oct)
Anti-aliasing filter	4.8 kHz (-18 dB/oct)
Gain	572 times
Dynamic range	$\pm 45 \mu\text{T}(\text{DC}),$
Averaging counts	$\pm 200 \text{nT}(\text{AC})$
Sampling frequency	8000

Table 4

Stimulus conditions.

Stimulus conditions	Values
Mode of delivery	Constant current (square pulse)
Intensity	10 mA (sub1, sub2), 8 mA (sub3)
Duration	0.2 ms
Stimulation rate	4.75 Hz

Table 5

Signal processing settings.

Signal processing settings	Values
Baseline correction	Offset subtraction with averaging pre-trigger 10 ms
Software high pass filter	20 Hz
Software low pass filter	300 Hz

measurements were made at 10 mA using a resistive load instead of a person. Therefore, these waveforms are thought to be the signals of human origin.

The contour map on the right side indicates the magnetic field distribution at the peak latency in the observation area illustrated at the top of Fig. 7. The contour map of the magnetic field was arranged as if looking at C3 from the front, with the parietal side at the top, left temporal side at the bottom, frontal side to the left, and occipital side to the right.

4. Discussion

4.1. Validity of the M20 component as the observed signal

On the contour map of the magnetic field at about 20 ms in latency shown in Fig. 7, a phase reversal was observed in all cases, wherein the signal was distributed from outward to inward of the head on the parietal side and inward to outward on the left temporal side. This suggests that this component originates from a current from the occipital to the frontal area near C3 and is considered as the M20 component originating from the primary somatosensory cortex. This is consistent with the physiological findings of preceding studies conducted using conventional SQUID-based MEGs [16–18], wherein the M20 component is estimated as a forward current dipole in the hand area of the primary somatosensory cortex localized in the posterior wall of the central sulcus.

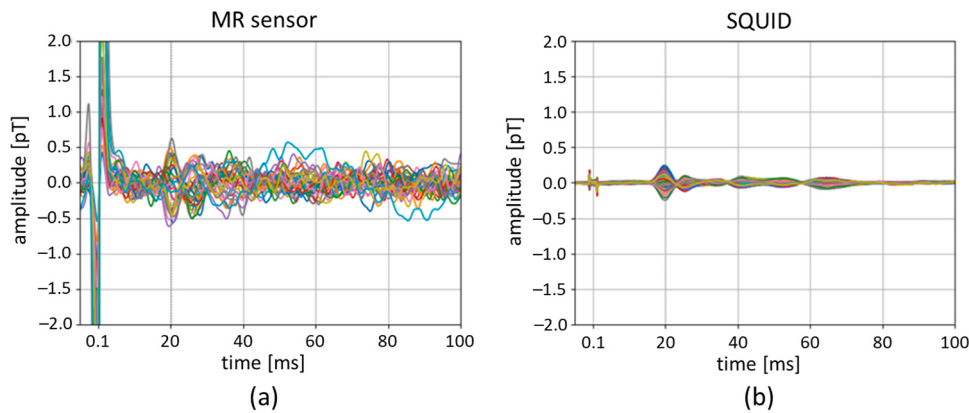


Fig. 5. Magnetic field waveforms obtained from Subject 1 recorded by the (a) MR sensors and (b) SQUID system.

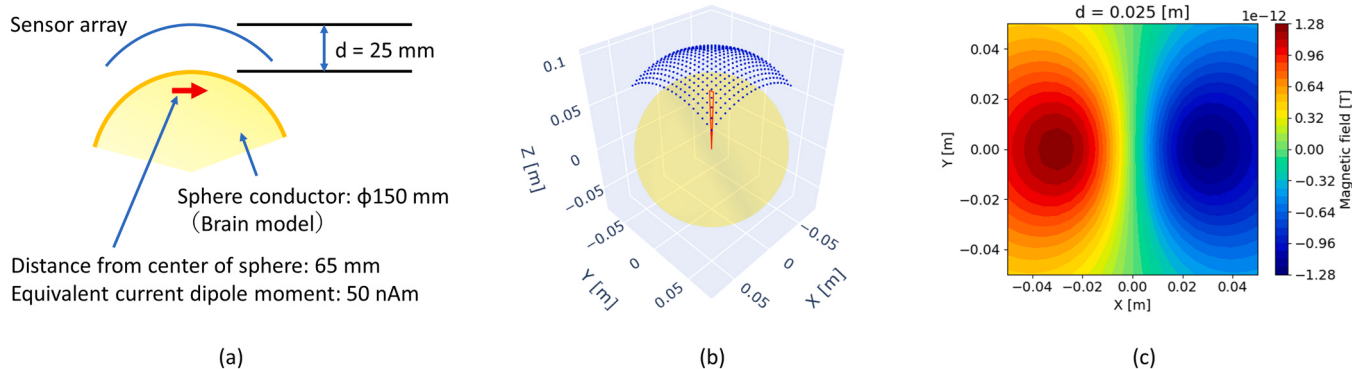


Fig. 6. Simulation of the magnetic field: (a) Simulation conditions based on [19], (b) Arrangement of the sensor array (Square configuration when viewed from the X-Y plane; sensors oriented normal to the spherical surface.), and (c) Magnetic field amplitude calculated in the Z direction at a height of 25 mm from the brain surface using the Sarvas formula. The potential range of maximum amplitude at a 30 mm interval is between 0.82 and 1.25 pT. The 25 mm corresponds to the sensitivity point of the MR sensors.

Fig. 5 shows a comparison of the SEF waveforms recorded by the MR sensor and SQUID for Subject 1. The difference in the M20 latency was 20.1 ms for the MR sensor and 19.9 ms for the SQUID, which was within the margin of error that could result from measurements recorded on different days. The maximum amplitude at the M20 component of the MR sensor was 606 fT, which is approximately 2.5-times that of the SQUID system (245 fT).

Furthermore, the amplitudes at M20 for Subject 2 were 536 fT, and for Subject 3, 1134 fT, respectively. We examined the validity of these amplitudes through a simulation (Fig. 6). As depicted in Fig. 6(a), a 50 nAm equivalent current dipole was positioned 65 mm away from the center of a conductor sphere with a diameter of 150 mm, based on [19]. The sensor array configuration, as shown in Fig. 6(b), was square when observed from the X-Y plane, with the sensors oriented perpendicular to the surface. Fig. 6(c) presents the magnetic field amplitude computed in the Z-direction at a height of 25 mm from the brain surface using Sarvas formula [20]. The potential range of maximum amplitude at a 30 mm pitch was determined to be between 0.82 and 1.25 pT. Therefore, amplitudes ranging from 536 to 1134 fT are considered reasonable for M20 amplitude.

4.2. M20 amplitude compared with that using SQUID sensors

In SEF measurements using SQUID sensors with similar filter conditions as described in references [17,21–23], the maximum amplitude of M20 was approximately 300 fT, as shown in Fig. 5. The amplitude of 725 fT (519–1134 fT) in this study was larger than that of the SEF measurements using SQUID sensors. This is because the SQUID sensor was located farther from the signal source owing to the thickness of the

vacuum layer in the cryostat, whereas the MR sensor was located closer to the signal source [7,24]. The magnetic field strength emitted by the magnetic source decreases as the square of the distance from the source.

4.3. Comparison with OPM

Several reports indicated that the SEF was detected by the MEG measurement based on OPM [7,25,26], another type of highly sensitive magnetic sensors recently applied to biomagnetic measurements other than SQUIDs, at a higher signal-to-noise ratio than that obtained in this study. For MR sensors, as utilized in this study, the sensitivity is 3 pT/Hz^{-0.5} at 10 Hz. Comparatively, OPMs have reported sensitivities of 10 fT/Hz^{-0.5} at 10 Hz [7], less than 15 fT/√Hz over the range of 3–100 Hz [25], and 30 fT/Hz^{-0.5} at 10 Hz [26]. The MR sensor still has the following superiorities compared with the OPM.

1) Low-cost production

MR sensors can be manufactured relatively inexpensively using existing manufacturing processes similar to those used for hard disk drive heads with an already established mass-production process. Despite installing a flux concentrator, the structure remains simple, and the manufacturing cost can be reduced.

2) Usable in a simple magnetically shielded room

Typically, OPMs necessitate either a zero-magnetic field environment or an internally compensated magnetic field, facilitated by coils integrated within the sensors [5,26–28]. Conversely, the MR sensor has a substantial dynamic range and is operable within a -32 dB magnetically shielded room (MSR), as used in this study. Even amidst the maximum environmental noise levels of 32 nT encountered in

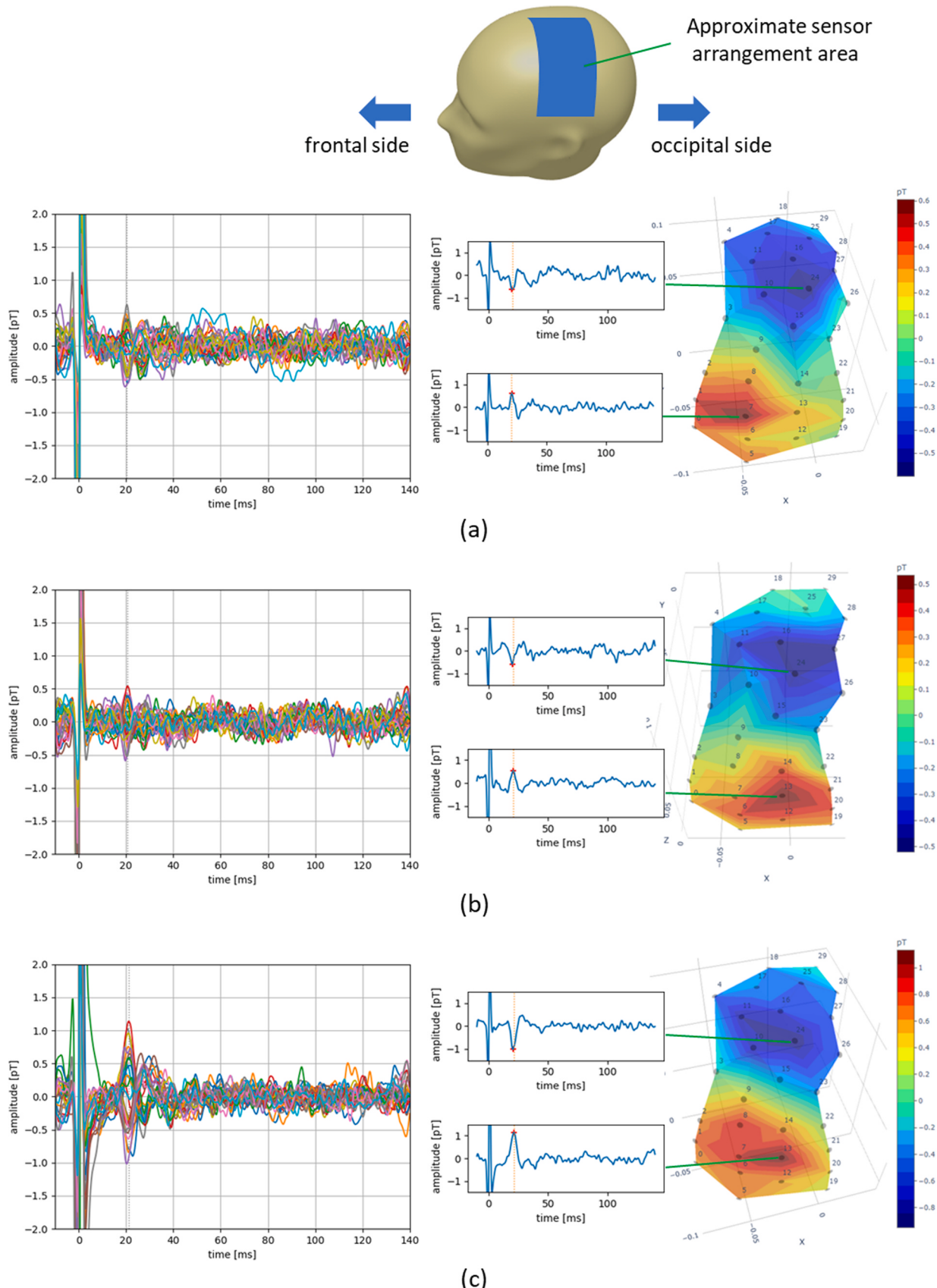


Fig. 7. (a), (b), and (c) Magnetic field waveforms and the contour map of the magnetic field obtained from subject 1, 2, and 3, respectively. Left side: Magnetic field waveforms. Center: Waveform with maximum amplitude of positive/negative peak around 20 ms. Right side: Isomagnetic field diagram and maximum amplitude waveforms.

the MSR—attributable to our urban location—MR sensors can successfully measure biomagnetic fields without necessitating any tuning, despite the high noise conditions. It should be noted, however, that OPM methodologies employing minimal magnetic shielding strategies, such as small magnetically shielded cylinders, have been documented. This suggests that the advantage of MR sensors in high noise environments may not be exclusive.

3) Low power consumption

Typical commercially available OPM products have a power consumption of 5 W (sensor head = 0.7 W) [28], whereas that of the MR sensor is 0.1 W (sensor head = approximately 0.025 W). The low power consumption of the sensor head is required for constructing multi-channel systems in future research.

As aforementioned, MR sensors are currently limited in their applications because of the restriction of magnetic field resolution; however, in certain cases, these sensors may be a promising option for realizing a reasonable MEG application device. For example, there are reports of neuromagnetic field measurements using SQUID sensors to measure the magnetic fields in the spinal cord and peripheral nerves [29,30]. MR sensors could be effective in measuring the SEF together with such magnetoneurographic (MNG) signals by SQUIDs simultaneously. To obtain the SEF signals by MR sensors, several thousands of repetitive electrical plural stimulations were necessary. However, in the case of simultaneous recording of the MEG and MNG signals especially from the spinal cord, it is acceptable as the signal detection from the spinal cord at the neck or back also requires averaging for several thousand times to achieve a sufficient signal-to-noise ratio, despite using SQUIDS, owing to the small signal intensity.

4.4. Comparison with preceding studies of multisite SEF measurements

There have already been reported cases wherein the M20 component of SEF has been measured using MR sensors [6]. In the previous study, multisite measurements were performed using a single sensor and by changing its position. However, in this study, the magnetic field distribution was demonstrated by simultaneously measuring the magnetic field using 30 sensor channels with the same performance. The advantages of simultaneous multisite measurements are that the measurement time is shortened to 1/(number of channels) and that the magnetic field source of spontaneous signals can be analyzed, and noise reduction can be applied using the multidimensionality of the signal space [31].

In another previous study [2] that measured the magnetic fields originating from the cerebrum using multiple sensors that could operate at room temperature, a whole-head mask tailored to a specific individual was produced using a 3D printer. However, the advantage of the array used in this study is that the sensor positions can be adjusted, thereby making it applicable to multiple subjects, and the position and orientation of each sensor were readily revealed by the measurement of the fiducial magnetic field from a spherical calibration coil after the SEF measurement.

4.5. Sensor placement with respect to the head surface for superior stability

In the third subject, the position of the marker coil attached to the head was estimated before and after the SEF measurement. The displacement of each marker coil before and after the measurement was below 0.72 mm, suggesting that the displacement in the head position during the measurement was negligible. In conventional SQUID-based MEGs, the helmet-shaped sensor array used to record MEG has a fixed size regardless of the subject, which may cause the head to move because of the gap between the head and sensor array. In contrast, the sensors in the sensor array used in this study maintained close contact with the head on both sides throughout the measurement, and the helmet-shaped sensor holder was fixed to a robust aluminum frame,

which provided excellent head position stability. Sensors that are inadequately fixed introduce artifacts caused by body motions when the head strikes the sensors. During our measurements, the sensor was firmly fixed to the sensor holder with screws to prevent it from being affected by body-motion artifacts.

4.6. Areas for improvement

The sensor array required time for sensor adjustment because this system needs to be fixed using four screws. This system may be improved such that it can be adjusted more easily and quickly.

In addition, the degree of contact of the sensor to the head was determined using the operator's hand and with verbal feedback from the subject. It would be better if the distance from the sensor to the scalp can be quantitatively understood.

5. Conclusion

Using a helmet-shaped 30-channel MR sensor array, the SEF of three healthy subjects was measured with a median nerve stimulation at the right wrist joint and averaging of 8000 epochs in the supine position in an MSR. In all cases, an obvious peak in the magnetic field waveforms was confirmed at a latency of approximately 20 ms. A phase inversion was observed around C3 in the international 10–20 system, which corresponded to the primary somatosensory cortex on the contour map of the magnetic field at the time of the peak. This indicated that the observed M20 component originated from the primary somatosensory cortex in a manner consistent with the conventional SEF measurement obtained by SQUID-based MEG.

The sensors were adjustable in the radial direction in the MR sensor array, making it possible to place the sensor in close contact with the subject's head. This contributed to the improved stability of the subject's head positioning and an improved signal-to-noise ratio.

The proposed MR sensor has the following advantages: a highly flexible layout, relatively low manufacturing costs and power consumption, and the ability to use simple MSR without requiring a zero-field environment. Moreover, it can be used as an “instantly-on” device without any parameter adjustment before measurement. The MR sensor was successfully used for simultaneous multipoint SEF measurements in humans despite its limited magnetic field resolution, indicating a promising method for realizing reasonably priced MEG devices.

Institutional Review Board Statement

This study was approved by the Ethical Review Committee of Tokyo Medical and Dental University Hospital. (Approval number: M2021-178)

CRediT authorship contribution statement

Jun Hashimoto: Methodology, Investigation. **Shigenori Kawabata:** Writing – review & editing, Validation, Methodology, Conceptualization. **Tetsuro Tatsuoka:** Writing – original draft, Software. **Yoshiaki Adachi:** Writing – review & editing, Validation, Methodology, Investigation, Conceptualization. **Tomohiko Shibuya:** Methodology, Investigation. **Atsushi Okawa:** Project administration. **Kensuke Sekihara:** Writing – review & editing, Validation. **Yuko Hoshino:** Writing – review & editing, Validation.

Declaration of Competing Interest

The authors declare the following financial interests/personal relationships which may be considered as potential competing interests: Tetsuro Tatsuoka reports a relationship with TDK Corporation that includes: employment. If there are other authors, they declare that they

have no known competing financial interests or personal relationships that could have appeared to influence the work reported in this paper.

Data Availability

Data will be made available on request.

References

- [1] M. Hämäläinen, R. Hari, R.J. Ilmoniemi, J. Knuutila, O.V. Lounasmaa, Magnetoencephalography—theory, instrumentation, and applications to noninvasive studies of the working human brain, *Rev. Mod. Phys.* 65 (1993) 413–497, <https://doi.org/10.1103/RevModPhys.65.413>.
- [2] R. Hari, S. Baillet, G. Barnes, R. Burgess, N. Forss, J. Gross, M. Hämäläinen, O. Jensen, R. Kakigi, F. Mauguière, N. Nakasato, A. Puce, G.-L. Romani, A. Schnitzler, S. Taulu, IFCN-endorsed practical guidelines for clinical magnetoencephalography (MEG), *Clin. Neurophysiol.* 129 (2018) 1720–1747, <https://doi.org/10.1016/j.clinph.2018.03.042>.
- [3] H.Y. Yu, N. Nakasato, M. Iwasaki, H. Shamoto, K. Nagamatsu, T. Yoshimoto, Neuromagnetic separation of secondarily bilateral synchronized spike foci: report of three cases, *J. Clin. Neurosci.* 11 (2004) 644–648, <https://doi.org/10.1016/j.jocn.2003.07.012>.
- [4] T. Uchiyama, J. Ma, Design and demonstration of novel magnetoencephalogram detectors, *IEEE Trans. Magn.* 55 (2019) 1–8, <https://doi.org/10.1109/TMAG.2019.2895399>.
- [5] R.M. Hill, E. Boto, M. Rea, N. Holmes, J. Leggett, L.A. Coles, M. Papastavrou, S. K. Everton, B.A.E. Hunt, D. Sims, J. Osborne, V. Shah, R. Bowtell, M.J. Brookes, Multi-channel whole-head OPM-MEG: Helmet design and a comparison with a conventional system, *NeuroImage* 219 (2020) 116995, <https://doi.org/10.1016/j.neuroimage.2020.116995>.
- [6] A. Kanno, N. Nakasato, M. Oogane, K. Fujiwara, T. Nakano, T. Arimoto, H. Matsuzaki, Y. Ando, Scalp attached tangential magnetoencephalography using tunnel magneto-resistive sensors, *Sci. Rep.* 12 (2022) 6106, <https://doi.org/10.1038/s41598-022-10155-6>.
- [7] E. Boto, S.S. Meyer, V. Shah, O. Alem, S. Knappe, P. Kruger, T.M. Fromhold, M. Lim, P.M. Glover, P.G. Morris, R. Bowtell, G.R. Barnes, M.J. Brookes, A new generation of magnetoencephalography: room temperature measurements using optically-pumped magnetometers, *NeuroImage* 149 (2017) 404–414, <https://doi.org/10.1016/j.neuroimage.2017.01.034>.
- [8] Pfeiffer, C., Ruffieux, S., Jönsson, L., Chukharkin, M.L., Kalaboukhov, A., Xie, M., Winkler, D., Schneiderman, J.F., 2019. A 7-channel high-Tc SQUID-based on-scalp MEG system. <https://doi.org/10.1101/534107>.
- [9] B. Riaz, C. Pfeiffer, J.F. Schneiderman, Evaluation of realistic layouts for next generation on-scalp MEG: spatial information density maps, *Sci. Rep.* 7 (2017) 6974, <https://doi.org/10.1038/s41598-017-07046-6>.
- [10] E. Boto, N. Holmes, J. Leggett, G. Roberts, V. Shah, S.S. Meyer, L.D. Muñoz, K. J. Mullinger, T.M. Tierney, S. Bestmann, G.R. Barnes, R. Bowtell, M.J. Brookes, Moving magnetoencephalography towards real-world applications with a wearable system, *Nature* 555 (2018) 657–661, <https://doi.org/10.1038/nature26147>.
- [11] Akushichi, T., Kameno, M., Kasajima, T., 2021. MAGNETIC SENSOR. PCT patent WO/2021/100252.
- [12] Y. Adachi, D. Oyama, M. Higuchi, G. Uehara, A spherical coil array for the calibration of whole-head magnetoencephalograph systems, *IEEE Trans. Instrum. Meas.* 72 (2023) 1–10, <https://doi.org/10.1109/TIM.2023.3265750>.
- [13] G. Crucu, M.J. Aminoff, G. Curio, J.M. Guerit, R. Kakigi, F. Mauguiere, P. M. Rossini, R.-D. Treede, L. Garcia-Larrea, Recommendations for the clinical use of somatosensory-evoked potentials, *Clin. Neurophysiol.* 119 (2008) 1705–1719, <https://doi.org/10.1016/j.clinph.2008.03.016>.
- [14] S. Erne, L. Narici, V. Pizzella, G. Romani, The positioning problem in biomagnetic measurements: a solution for arrays of superconducting sensors, *IEEE Trans. Magn.* 23 (1987) 1319–1322, <https://doi.org/10.1109/TMAG.1987.1064889>.
- [15] Y. Adachi, J. Kawai, Y. Haruta, M. Miyamoto, S. Kawabata, K. Sekihara, G. Uehara, Recent advancements in the SQUID magnetospinogram system, *Supercond. Sci. Technol.* 30 (2017) 063001, <https://doi.org/10.1088/1361-6668/aa66b3>.
- [16] T. Kawamura, N. Nakasato, K. Seki, A. Kanno, S. Fujita, S. Fujiwara, T. Yoshimoto, Neuromagnetic evidence of pre- and post-central cortical sources of somatosensory evoked responses, *Electroencephalogr. Clin. Neurophysiol. /Evoked Potentials Sect.* 100 (1996) 44–50, [https://doi.org/10.1016/0168-5597\(95\)00217-0](https://doi.org/10.1016/0168-5597(95)00217-0).
- [17] M. Scherg, H. Buchner, Somatosensory evoked potentials and magnetic fields: separation of multiple source activities, *Physiol. Meas.* 14 (1993) A35, <https://doi.org/10.1088/0967-3334/14/4A/006>.
- [18] M. Iwasaki, N. Nakasato, A. Kanno, K. Hatanaka, K. Nagamatsu, Y. Nagamine, T. Yoshimoto, Somatosensory evoked fields in comatose survivors after severe traumatic brain injury, *Clin. Neurophysiol.* 112 (2001) 205–211, [https://doi.org/10.1016/S1388-2457\(00\)00506-X](https://doi.org/10.1016/S1388-2457(00)00506-X).
- [19] D. Oyama, Y. Adachi, M. Yumoto, I. Hashimoto, G. Uehara, Dry phantom for magnetoencephalography —configuration, calibration, and contribution, *J. Neurosci. Methods* 251 (2015) 24–36, <https://doi.org/10.1016/j.jneumeth.2015.05.004>.
- [20] J. Sarvas, Basic mathematical and electromagnetic concepts of the biomagnetic inverse problem, *Phys. Med. Biol.* 32 (1987) 11, <https://doi.org/10.1088/0031-9155/32/1/004>.
- [21] I. Hashimoto, T. Kimura, M. Tanosaki, Y. Iguchi, K. Sekihara, Muscle afferent inputs from the hand activate human cerebellum sequentially through parallel and climbing fiber systems, *Clin. Neurophysiol.* 114 (2003) 2107–2117, [https://doi.org/10.1016/S1388-2457\(03\)00233-5](https://doi.org/10.1016/S1388-2457(03)00233-5).
- [22] N. Nakasato, K. Seki, T. Kawamura, S. Ohtomo, A. Kanno, S. Fujita, K. Hatanaka, S. Fujiwara, T. Kayama, A. Takahashi, H. Jokura, T. Kumabe, H. Ikeda, K. Mizoi, T. Yoshimoto, Cortical mapping using an MRI-linked whole head MEG system and presurgical decision making, *Electroencephalogr. Clin. Neurophysiol. Suppl.* 47 (1996) 333–341.
- [23] M. Ishida, K. Jin, Y. Kakisaka, A. Kanno, R. Kawashima, N. Nakasato, Awake state-specific suppression of primary somatosensory evoked response correlated with duration of temporal lobe epilepsy, *Sci. Rep.* 10 (2020) 15895, <https://doi.org/10.1038/s41598-020-73051-x>.
- [24] J. Ilvanainen, M. Stenroos, L. Parkkonen, Measuring MEG closer to the brain: performance of on-scalp sensor arrays, *NeuroImage* 147 (2017) 542–553, <https://doi.org/10.1016/j.neuroimage.2016.12.048>.
- [25] N. An, F. Cao, W. Li, W. Wang, W. Xu, C. Wang, M. Xiang, Y. Gao, B. Sui, A. Liang, X. Ning, Imaging somatosensory cortex responses measured by OPM-MEG: Variational free energy-based spatial smoothing estimation approach, *iScience* 25 (2022) 103752, <https://doi.org/10.1016/j.isci.2022.103752>.
- [26] A. Borna, T.R. Carter, J.D. Goldberg, A.P. Colombo, Y.-Y. Jau, C. Berry, J. McKay, J. Stephen, M. Weisend, P.D.D. Schwindt, A 20-channel magnetoencephalography system based on optically pumped magnetometers, *Phys. Med. Biol.* 62 (2017) 8909, <https://doi.org/10.1088/1361-6560/aa93d1>.
- [27] K. He, S. Wan, J. Sheng, D. Liu, C. Wang, D. Li, L. Qin, S. Luo, J. Qin, J.-H. Gao, A high-performance compact magnetic shield for optically pumped magnetometer-based magnetoencephalography, *Rev. Sci. Instrum.* 90 (2019) 064102, <https://doi.org/10.1063/1.5066250>.
- [28] J. Osborne, J. Orton, O. Alem, V. Shah, Fully integrated standalone zero field optically pumped magnetometer for biomagnetism, in: *Steep Dispersion Engineering and Opto-Atomic Precision Metrology XI*. Presented at the *Steep Dispersion Engineering and Opto-Atomic Precision Metrology XI*, SPIE, 2018, pp. 89–95, <https://doi.org/10.1117/12.2299197>.
- [29] Y. Adachi, S. Kawabata, J. Hashimoto, Y. Okada, Y. Naijo, T. Watanabe, Y. Miyano, G. Uehara, Multichannel SQUID magnetoneurograph system for functional imaging of spinal cords and peripheral nerves, *IEEE Trans. Appl. Supercond.* 31 (2021) 1–5, <https://doi.org/10.1109/TASC.2021.3056492>.
- [30] S. Sumiya, S. Kawabata, Y. Hoshino, Y. Adachi, K. Sekihara, S. Tomizawa, M. Tomori, S. Ishii, K. Sakaki, D. Ukegawa, S. Ushio, T. Watanabe, A. Okawa, Magnetospinography visualizes electrophysiological activity in the cervical spinal cord, *Sci. Rep.* 7 (2017) 2192, <https://doi.org/10.1038/s41598-017-02406-8>.
- [31] C. Cai, H. Kang, H.E. Kirsch, D. Mizuiri, J. Chen, A. Bhutada, K. Sekihara, S. Nagarajan, Comparison of DSSP and tSSS algorithms for removing artifacts from vagus nerve stimulators in magnetoencephalography data, *J. Neural Eng.* 16 (2019) 066045, <https://doi.org/10.1088/1741-2552/ab4065>.